Theoretical and Experimental Salvation of Nano Copper Sulfate Interacted with 18-crown-6 in Water

G. Sanad, Sameh; Shimaa, Abdel Halim *+; I. Ali, Laila

Department of Chemistry, Faculty of Education, Ain Shams University, Roxy 11711, Cairo, EGYPT

ABSTRACT: *Theoretical study of the electronic structure, NonLinear Optical (NLO) properties, and natural bonding orbital (NBO) analysis of 18-crown-6 were investigated using Density Functional Theory (DFT) calculations at the B3LYP/6-311G (d,p) level of theory. The optimized structure is a nonlinear compound as indicated from the dihedral angles. Natural bonding orbital analysis has been analyzed in terms of the hybridization of each atom, natural charges (Core, Valence, and Rydberg), bonding and antibonding orbital's second-order perturbation energy ($E^{(2)}$). The calculated E_{HOMO} and E_{LUMO} energies of the title molecule can be used to explain the charge transfer in the molecule and to calculate the global properties; the chemical hardness (η), softness (S), global electrophilicity index (ω), and electronegativity (χ). The NLO parameters: static dipole moment (μ), polarizability (α), anisotropy polarizability ($\Delta\alpha$), first-order hyperpolarizability (β_{tot}) and third-order hyperpolarizability (γ)), of the studied molecule have been calculated at the same level of theory. The Molecular Electrostatic Potential (MEP) and ElectroStatic Potential (ESP) for the title molecule were investigated and analyzed. Also, the electronic absorption spectra were discussed by time-dependent density functional theory (TD-DFT) calculations in ethanol and water solvents. From the experimental conductance measurements, the association thermodynamic parameters (K_A, ΔG_A, ΔH_A, and ΔS_A) and complex formation thermodynamic parameters (K_f, ΔG_f, ΔH_f, and ΔS_f) of nano-$CuSO_4$ in presence of 18-crown-6 as a ligand in 10% ethanol-waterer solvents at different temperatures (298.15, 303.15, 308.15 and 313.15K) were applied and calculated.*

KEYWORDS: *DFT/TD-DFT; NLO and NBO analysis; UV-spectra; Association parameters; Formation parameters; Nano-$CuSO_4$; 18-crown-6.*

INTRODUCTION

Crown ethers were discovered by *Pederson* in 1967 [1] and became the first synthetic ligands to demonstrate selectivity for metal ions. Crown ethers have a hydrophilic cavity delineated by a lipophilic portion of the molecule. Crown ethers have been studied extensively [2], and it was determined that their structures were comparable to certain antibiotics like valinomycin [3] or enunciation[4]. These structural similarities led to the use of crown ethers as reference models to study the binding and delivery mechanism of these antibiotics to their target sites [5]. Gas-phase conformational analyses of 18c6 [6-8] were reported previously. However, consideration of solvent-solute interactions [9] is essential, and the distributional treatment of

** To whom correspondence should be addressed.*
+ E-mail: shimaaquantum@ymail.com
1021-9986/2020/1/11-30 20/$/7.00

thermodynamic properties in each phase will substantially improve the results and the accuracy of conclusion of the 'Guest–Host' interaction. Since the seminal work on Self-Consistent Reaction Fields (SCRF) by Onsager [10], there has been a tremendous amount of research done on the theoretical framework for solution phase studies [11]. This implicit solvation model approach is popular because it allows the calculation of the properties of a molecule in solution without prohibitively expensive computational cost. Even with the reduced computational cost, the geometry optimization of relatively large molecule such as crown ether requires significant amount of computational resource. The empirical geometrical parameters of solute in aqueous solution could not only provide the benchmark to the theory but also assist the reduction of computational resource [12].

The NLO properties depend on the extent of Charge Transfer (CT) interaction across the conjugative paths and the electron transfer ability of an aromatic ring and on its Ionization Potential (IP) and electron affinity (EA) [13, 14]. Linear polarizability $\langle \Delta\alpha \rangle$ and first order hyperpolarizability $\langle \beta \rangle$ are required for the rational design of optimized materials for photonic devices such as electrooptic modulators and all-optical switches [15, 16]. Natural Bond Orbital (NBO) analysis was originated as a technique for studying hybridization and covalence effects in polyatomic wave functions. The work of *Foster* and *Winhold* [17] was extended by *Reed et al.*, [18] who employed NBO analysis that exhibited particularly H-bonded and other strongly bound van der Waals complexes. The filled NBOs σ of the "natural Lewis structure" is well adapted to describing covalence effects in molecules [18]. However, the general transformation to NBOs also leads to orbital's that are unoccupied in the formal Lewis structure and that may be used to describe noncovalent effects. the symbols σ and σ^* are used in a generic sense to refer to filled and unfilled orbital's of the formal Lewis structure, though the former orbital's may actually be core orbital's (*CR*), lone pairs (*LP*), σ or π bonds (σ, π), and so forth, and the latter may be σ or π antibonds (σ^*, π^*), extravalenceshell Rydberg (*RY**) orbital's. In these study our contribution here is to shed more light on the geometric structure (bond lengths, bond angles and dihedral angles), ground state properties of 18-crown-6 using Density Functional Theory (DFT-B3LYP) and basis set 6-311G (d,p), Natural Bonding Orbital's (NBO) and NonLinear Optical (NLO) analysis are performed to identify and characterize the forces that govern the structure of the title molecule. The results from natural bonding orbital analysis have been analyzed in terms of the hybridization of each atom, natural charges (Core, Valence and Rydberg), bonding and antibonding orbital's second order perturbation energy ($E^{(2)}$), exact configurations and Lewis and non-Lewis electrons. In addition to investigate the effect of solvent polarity on the observed spectra and hence, predicting the relative stabilities, extent of charge transfer character and assignment of the observed electronic transitions bands as localized, delocalized and/or of Charge Transfer (CT) has been facilitated by Density Functional Theory (DFT) and Time-Dependent Density Functional Theory (TD-DFT) calculations. The electronic structure of molecules usually manifests itself in the electronic absorption and emission spectra. This manifestation enables the detailed understanding of the forces that govern the electronic structure of the studied compound 18-crown-6.

Copper sulfate is a fungicide material. Some fungi able to elevate levels of copper ions. Algae can be controlled with small copper sulfate concentration. Copper sulfate inhibits growth of bacteria. Copper sulfate can form cause cell death which through apoptosis and necrosis [19, 20].

EXPERIMENTAL SECTION

Preparation of materials

In 5 ml of the nano-$CuSO_4$ solution (1.0×10^{-3} M) and solution of 18-crown-6 (1.0×10^{-4} M) were placed in the titration cell, thermostated at the preset temperature and the conductance of the solution was measured after the solution reached thermal equilibrium. Then, a known amount of solvent was added in a stepwise manner using a calibrated micropipette. The conductance of the solution was measured after each addition until the desired constant reading was achieved. The specific conductance values were recorded using conductivity bridge JENCO – 3173 COND. with a cell constant equal to 1. The temperature was adjusted at 298.15, 303.15, 308.15 and 313.15K [21, 22].

Computational method

Calculations have been performed using Khon-Sham's Density Functional Theory (DFT) method subjected to the gradient-corrected hybrid density

functional B3LYP method [23]. This function is a combination of the Becke's three parameters non-local exchange potential with the non-local correlation functional of *Lee et al* [24]. For each structure, a full geometry optimization was performed using this function [24] and the 6-311G (p,d) basis set [25] as implemented by Gaussian 09 package [26]. All geometries were visualized either using GaussView 5.0.9 [27] or chemcraft 1.6 software packages. No symmetry constrains were applied during the geometry optimization. Also, the total static dipole moment (μ), $\langle\Delta\alpha\rangle$, $\langle\beta\rangle$ and $\langle\gamma\rangle$, values were calculated by using the following equations [28-30]:

$$\mu = \left(\mu_x^2 + \mu_y^2 + \mu_z^2\right)^{1/2} \quad (1)$$

$$\langle\alpha\rangle = 1/3\left(\alpha_{xx} + \alpha_{yy} + \alpha_{xzz}\right)$$

$$\Delta\alpha = \left(\frac{\left(\alpha_{xx} - \alpha_{yy}\right)^2 + \left(\alpha_{yy} - \alpha_{zz}\right)^2 + \left(\alpha_{zz} - \alpha_{xx}\right)^2}{2}\right)^{1/2}$$

$$\langle y\rangle = (1/5)\left[\gamma_{xxxx} + \gamma_{yyyy} + \gamma_{zzzz} + 2\left(\gamma_{xxyy} + \gamma_{xxzz} + \gamma_{yyzz}\right)\right]$$

$$\langle\beta\rangle = \left(\beta_x^2 + \beta_y^2 + \beta_z^2\right)^{1/2}$$

Where

$$\beta_x = \beta_{xxx} + \beta_{xyy} + \beta_{xzz} \quad (2)$$

$$\beta_y = \beta_{yyy} + \beta_{xxy} + \beta_{yzz}$$

$$\beta_z = \beta_{zzz} + \beta_{xxz} + \beta_{yyz}$$

By using HOMO and LUMO energy values for a molecule, electronegativity, and chemical hardness can be calculated as follows: $\chi = (I + A)/2$ (electronegativity), $\eta = (I - A)/2$ (chemical hardness), $\omega = \mu^2/2\eta$ (electrophilicity), and $S = 1/2\eta$ (chemical softness) where I and A are ionization potential and electron affinity, and $I = -E_{HOMO}$ and $A = -E_{LUMO}$, respectively [31,32]. The population analysis has also been performed by the natural bond orbital method [33] at B3LYP/6-311G (d,p) level of theory using natural bond orbital (NBO) under Gaussian 09 program package. The second-order Fock matrix was used to evaluate the donor-acceptor interactions in the NBO basis [34]. The interactions result in a loss of occupancy from the localized NBO of the idealized Lewis structure into an empty non-Lewis orbital. For each donor (i) and acceptor (j), the stabilization energy $E^{(2)}$ associated with the delocalization $i \rightarrow j$ is estimated as

$$E^{(2)} = \Delta E_{ij} = q_i\left(F(ij)^2 / \varepsilon_j - \varepsilon_i'\right) \quad (3)$$

Where q_i is the donor orbital occupancy, ε_i and ε_j are diagonal elements and $F(ij)$ is the off-diagonal NBO Fock matrix element. The conversion factors for α, β, γ, and HOMO and LUMO energies in atomic and cgs units: 1 atomic unit (a.u.) = 0.1482×10^{-24} electrostatic unit (esu) for polarizability; 1 a.u. = 8.6393×10^{-33} esu for first hyperpolarizability; and third-order hyperpolarizability $\langle\gamma\rangle$; 1 a.u. = 27.2116 eV (electron volt) for HOMO and LUMO energies.

RESULTS AND DISCUSSION

Association thermodynamic parameters

The association constants for nano-$CuSO_4$ in the presence of ligand 18-crown-6 in ethanol and water at different temperatures (298.15, 303.15, 308.15 and 313.15K) were calculated by using equation (4) [35-40].

$$K_A = \Lambda 0\left(\Lambda_0 - S(Z)A_m\right) \quad (4)$$

$$C_m\Lambda_m S(Z)^{2\gamma\pm2}$$

Where (Λ_m, Λ_0) are the molar and limiting molar conductance of nano- $CuSO_4$ in presence of ligand respectively, C_m is the molar concentration of nano-$CuSO_4$, S(Z) is Fouss – Shedlovsky factor, equal with unity for strong electrolytes, $\gamma_\pm$ is the mean activity coefficient.

The association constants, in presence of 18-crown-6 for nano- $CuSO_4$ at different temperatures are tabulated in Table 1, indicating that the association constants increase with increase the temperature. Free energies, enthalpies and entropies of association for nano- $CuSO_4$ in presence of 18-crown-6 at different temperatures are estimated in Table 2. The free energies of association increase in negativity with increasing of temperature. Negative free energies indicate the spontaneous character of the process.

The relation between molar conductance (Λ_m) and square root of concentration ($C^{1/2}$) for nano- $CuSO_4$ in presence of 18-crown-6 at different temperatures in Fig. 1, show the inversely relationship between the molar conductance and square root of concentration. Also, the molar conductance decreases with increase the temperature.

Table 1: Association constants at different temperatures for nano- $CuSO_4$ in presence of 18-Crown-6 (10% ethanol-90% water).

T (K)	C	$C^{1/2}$	Λ_m	Λ_0	Log $\gamma_\pm$	$\gamma_\pm$	K_A
298.15	9.091×10^{-5}	0.0095	729.2	1600	-0.0048	0.977	30195.64
303.15	9.091×10^{-5}	0.0095	1007.5	3000	-0.0048	0.977	67862.32
308.15	9.091×10^{-5}	0.0095	499.3	1100	-0.0048	0.977	30544.03
313.15	9.091×10^{-5}	0.0095	420.196	960	-0.0048	0.977	33822.27

Table 2: Free energies, enthalpies and entropies of association for nano- CuSO4 in presence of 18-Crown-6 at different temperatures (10% ethanol-90% water).

T(K)	ΔG_A	ΔH_A	$T\Delta S_A$	ΔS_A
298.16	-25.5756	132.767	158.3426	0.5311
303.16	-28.0459	132.767	160.8129	0.0053
308.16	-26.4628	132.767	159.2298	0.5167
313.16	-27.1576	132.767	159.9246	0.5107

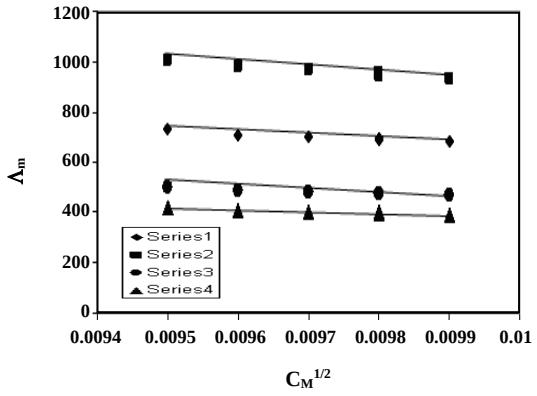

Fig. 1: The relation between Λ_m and $C^{1/2}$ for nano- $CuSO_4$ in presence of 18-crown-6 at different temperatures (10% ethanol-90% water).

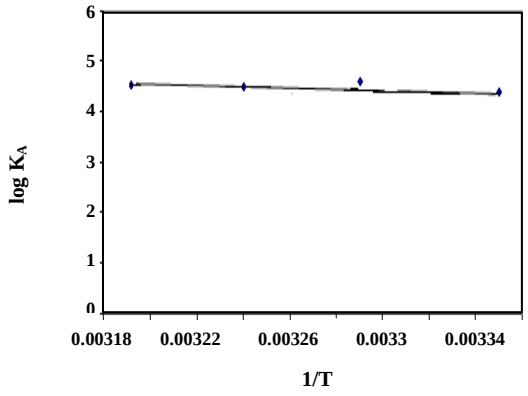

Fig. 2: The relation between log K_A and 1/T for nano- $CuSO_4$ in presence of 18-crown-6 at different temperatures (10% ethanol-90% water).

The relation between log K_A and 1/T in presence of 18-crown-6 for nano- $CuSO_4$ is shown in Fig. 2.

Formation constants, free energies, enthalpies and entropies of formation for nano- $CuSO_4$ in presence of 18-crown-6 at different temperatures are estimated in Table 3. Table 3, showing that the formation constants and free energies in case of (1:2) metal to ligand is more favourable than (1:1) metal to ligand.

Formation thermodynamic parameters

The relations between molar conductance (Λ_m) and the molar ratio of metal to ligand (M/L) indicating the formation of 1:2 and 1:1 stoichiometric complexes. The formation constants (K_f) for the complexes were calculated for each type of complexes 1:2 and 1:1 (M:L) by using equation (5) [41-44].

$$K_f = \frac{\Lambda_M - A_{obs}}{(\Lambda_{obs} - \Lambda_{mL})[L]} \quad (5)$$

Where Λ_M is the limiting molar conductance of the salt alone, Λ_{obs} is the molar conductance of solution during titration and Λ_{ML} is the molar conductance of the complex. By drawing the relation between the molar conductance (Λ_m) and the molar ratio of metal to ligand (C_M/C_L) concentrations, the figures which obtained

Table 3: Formation constants, free energies, enthalpies and entropies of formation for nano- $CuSO_4$ in presence of 18-Crown-6 at different temperatures (10% ethanol-90% water).

TEMP	M:L	K_f	ΔG_f	ΔH_f	ΔS_f
298.15	1:2	8484.973	-22.4283	-137.5492	-0.3861
	1:1	353895.6	-31.678	-17.7195	0.0468
303.15	1:2	14732.51	-24.1954	-137.5492	-0.3739
	1:1	58391.38	-27.667	-17.7195	0.0328
308.15	1:2	6442.986	-22.4751	-137.5492	-0.3734
	1:1	52490.07	-27.2426	-17.7195	0.0309
313.15	1:2	6619.376	-22.9101	-137.5492	-0.3661
	1:1	46770.35	-28.0017	-17.7195	0.0328

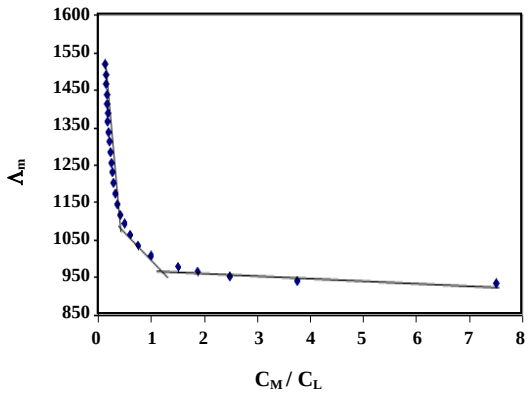

Fig. 3: The relation between Λ_m and C_M/C_L at 298.15K for nano- $CuSO_4$ in presence of 18-crown-6 (10% ethanol-90% water).

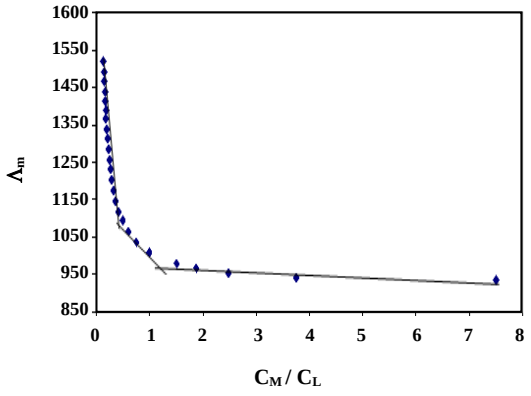

Fig. 4: The relation between Λ_m and C_M/C_L at 303.15K for nano- $CuSO_4$ in presence of 18-crown-6 (10% ethanol-90% water).

indicating the formation of 1:2 and 1:1stoichiometric complexes. The relation between Λ_m and C_M/C_L at different temperatures (298.15, 303.15, 308.15 and 313.15K) for nano- $CuSO_4$ in presence of 18-crown-6 in ethanol-water mixed solvents are shown in Figs. (3-6). Figs. (7 and 8).

show the relation between log K_f and 1/T when M:L is 1:2 and 1:1 respectively for nano- $CuSO_4$ in presence of 18-crown-6. Fig. 9. TEM for nano- $CuSO_4$ (a-d). Fig.9. In all images (a-d) measured by using JEOL HRTEM – JEM 2100 (JAPAN) show that TEM of CuSO4 obtained in ethanol are irregular spheres in the form of cylinders. The diameter in the range of 10-77.86 nm. The small sizes in the range between 10, 12.05 to 20.76 nm are collected to give bigger sizes till 77.86 nm (a-c). These different sizes were proved also by x- ray diffraction which gave crystal sizes in the same order (d). The non homogeneity in sizes for Nano copper sulfate need controlling during the primary preparation of the samples.

Ground state properties

The total energy (E_T), energy of highest occupied molecular orbital (E_{HOMO}), energy of lowest unoccupied molecular orbital (E_{LUMO}), energy gap (E_g) and dipole moment (μ) of of the studied compound 18-crown-6 are presented in Table 4. The optimized structure of the title molecule is obtained using the B3LYB/6-311G (p,d) level, numbering system, net charge, vector of dipole moment and the charge density maps of HOMO and LUMO are presented in Fig. 10.

The ionization energy, I.E, of compound 18-crown-6 which measures the donating property (oxidation power)

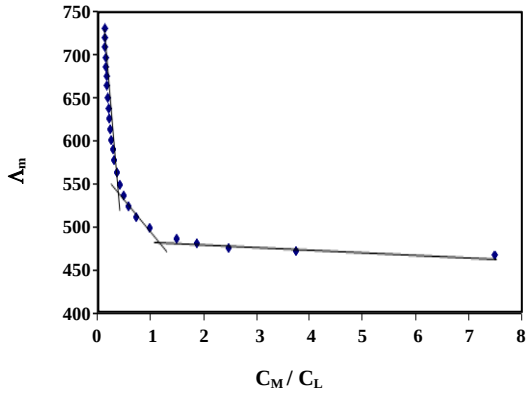

Fig. 5: The relation between Λ_m and C_M/C_L at 308.15K for nano- $CuSO_4$ in presence of 18-crown-6 (10% ethanol-90% water).

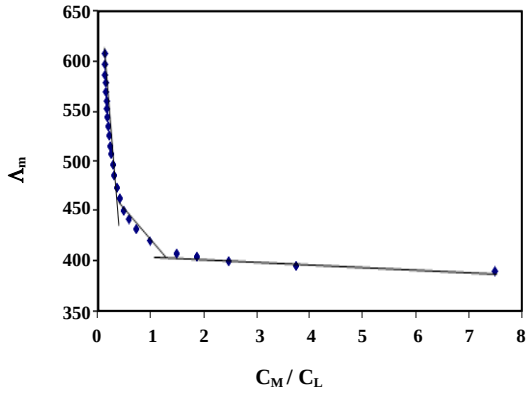

Fig. 6: The relation between Λ_m and C_M/C_L at 313.15K for nano- $CuSO_4$ in presence of 18-crown-6 (10% ethanol-90% water).

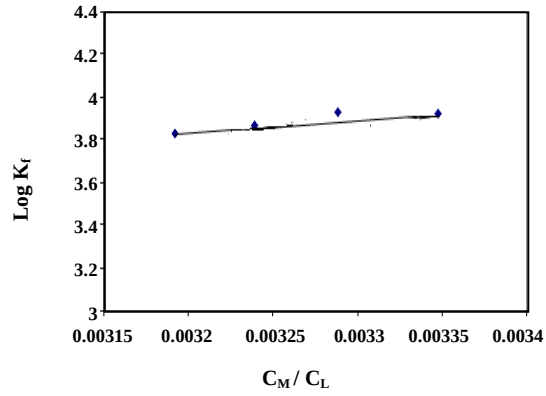

Fig. 7: Relation between $\log K_f$ and 1/T when M:L is 1:2 for nano- $CuSO_4$ in presence of 18-crown-6 (10% ethanol-90% water).

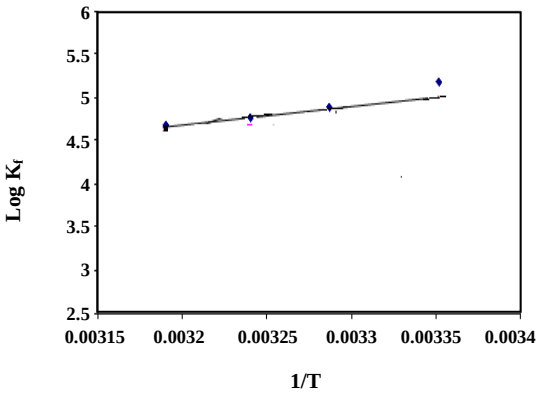

Fig. 8: Relation between $\log K_f$ and 1/T when M:L is 1:1 for nano- $CuSO_4$ in presence of 18-crown-6 (10% ethanol-90% water).

is 7.37 eV (c.f. Table 4). Also the electron affinity (E.A) which measures the accepting property (reducing power) is 2.30 eV. So the calculated energy gaps, (Eg), which measure the chemical activity, of compound free 18-crown-6 is 5.07 eV (≈ 117 kcal). Finally, the theoretically computed dipole moment (μ), which measures the polarity or charge separation over the title molecule, is 1.25 D.

Geometric Structure

The optimized geometric parameters (bond lengths, bond angles and dihedral angles) of the title molecules using B3LYP/6-311G (d,p) level of theory are listed in Table 5, and are compared with the available x-ray experimental data 45. The observed bond lengths of C_1-C_8, C_1-O_{11} and C_1-H_{24} in 18-crown-6 are 1.487 Å, 1.422 Å and 1.091 Å respectively, while the obtained theoretical values are 1.513 Å, 1.413 Å and 1.099 Å respectively [45]. The computed bond angles of $<C_3O_{10}C_4$, $<O_{11}C_2H_{25}$, $<C_1H_{23}H_{24}$, and $<C_2C_3H_{27}$ are 110.83°, 108.04°, 108.04° and 110.44° respectively, while the experimental values are 116.93°, 107.64°, 107.54° and 110.44° respectively. In conclusion, the bond lengths and angles calculated by B3LYP methods are in good agreement with the experimental values. The Mullikan net charge observed on active centers O1, O2, O3, O4, O5, O6 and Cu are -0.356, -0.356, -0.359, -0.360, -0.360, -0.468 and 0.065 respectively. The most stable geometry of the studied compound is non-planar structure as indicated from the dihedral angles (c.f. Table 5).

Table 4: Total energy, energy of HOMO and LUMO, energy gap and dipole moment of 18-Crown-6 computed at the B3LYP/6-311G (d,P) level of theory.

Compounds	E_T (au)	E_{HOMO} (eV)	E_{LUMO} (eV)	E_{gap} (eV)	μ (Debye)
18-Crown-6	-2563.6331	-7.3709	-2.2984	5.0725	1.2479

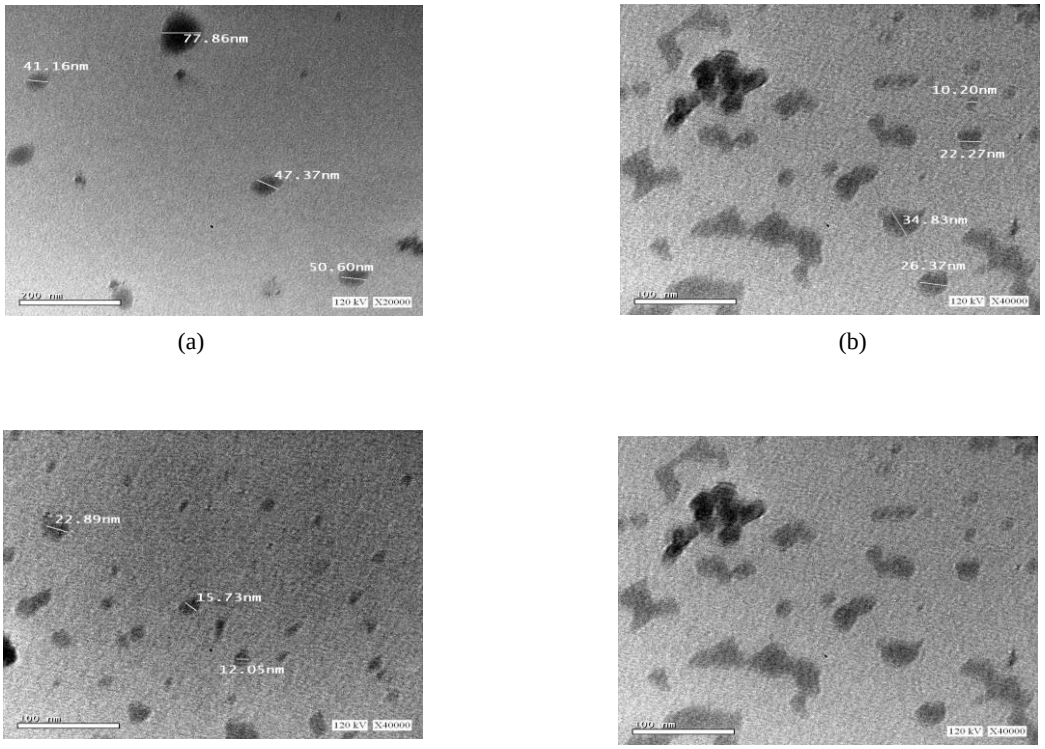

Fig. 9: TEM for nano- $CuSO_4$ (a-d).

Natural Bonding Orbital (NBO) analysis

The NBO analysis provides an efficient method for studying intra-and intermolecular bonding and interaction among bonds, and also enables a convenient basis for investigating charge transfer or conjugative interaction in molecular systems [46]. The larger the interacting stabilization energy $E^{(2)}$ value, the more intensive is the interaction between electron donors and the greater the extent of conjugation of the whole system. Delocalization of electron density between occupied Lewis type (bond or lone pair) NBO orbital's and formally unoccupied (antibonding or Rydberg) non Lewis NBO orbital's correspond to a stabling donor-acceptor interaction [47, 48]. NBO analysis was performed on the title molecule at the DFT/B3LYP/6-311G (d,p) level in order to elucidate the intra molecular rehybridization and delocalization of electron density within the molecule. The molecular interaction is formed by the orbital overlap between σ (C-C) and σ∗ (C-C) bond orbital which results that intramolecular charge (ICT) is causing stabilization of the system. These interactions are observed as increase in electron density (ED) in C-C antibonding orbital that weakens the respective bonds. The electron density of conjugated double as well as the single bond of the conjugated ring (≈ 1.9e) clearly demonstrates strong delocalization inside the molecule [49].

Donor-acceptor bonding in title molecules

The perturbation energies of donor-acceptor interactions and type of each bonding and antibonding

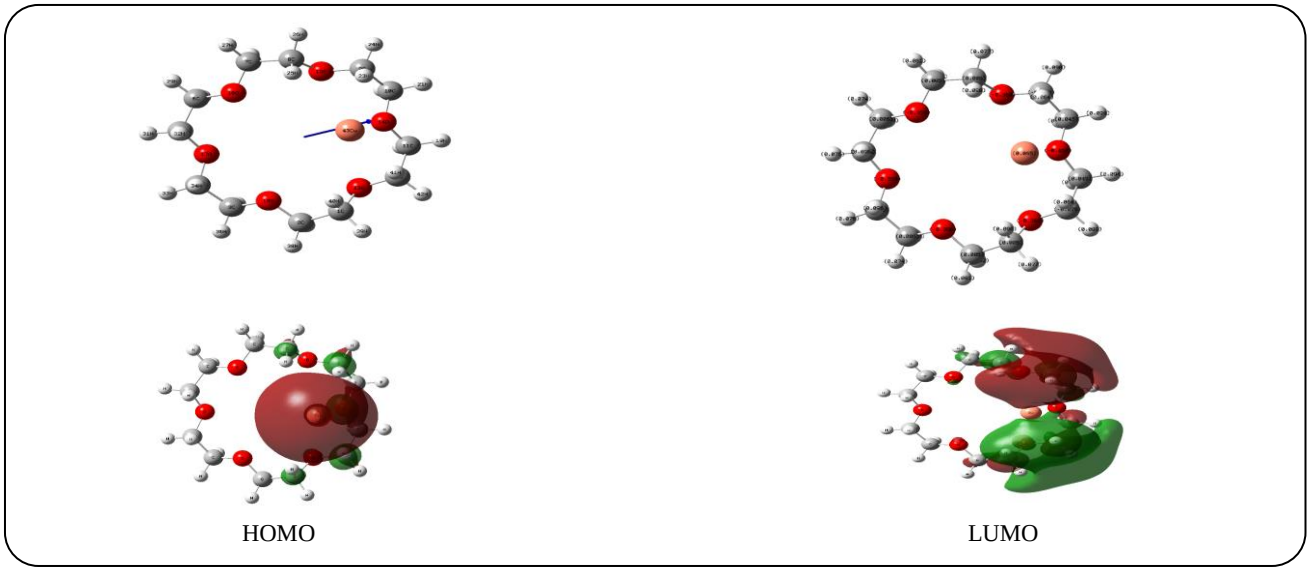

Fig. 10: Optimized geometry, numbering system, net charge, vector of dipole moment, HOMO and LUMO for 18-crown-6 using B3LYP/6-311G (d,p).

orbital's, Fock-matrix element between donor and acceptor orbital's, occupancy of donor Lewis-type NBO's, hybridization and % AO of the studied molecule using B3LYP/6-311G (d,p) are presented in Tables (6 and 7). In our title molecule LP (2) O_{15} → σ∗ (C_9-H_{24}) has 4.36 kJ/mol, LP (2) O_{16} → σ ∗ (C_7-H_{27}) has 3.99 kJ/mol and LP (2) O_{13} → σ ∗ (C_1-H_{39}) has 3.21 kJ/mol. Hence, they give stronger stabilization to the structure. From Table 7 ; it is noted that the maximum occupancies 0.99192, 0.99186, 0.96592, 0.95904 are obtained for σ (C_2-H_{38}), σ (C_4-H_{33}), LP (2) O_{14} and LP (2) O_{15}, respectively. Therefore these bonds are essentially controlled by the sp- and p-character of the hybrid orbital's (c.f. Table 7).

The calculated natural hybrids on each atoms and occupancies are given in Table 7. As seen from Table 7, the σ (C_{12}-H_{42}) bond is formed from $sp^{3,13}$ hybrids on carbon (which is a mixture of 24.20% *s*, 75.73% *p*, and 0.07% *d* atomic orbital's). On the other hand, σ (C_4-H_{33}) bond is formed from $sp^{3,\ 23}$ hybrids on carbon (which is a mixture of 23.65% *s*, 76.28% *p*, and 0.08% *d* atomic orbital's). LP (2) O_{14} is formed from $p^{1.00}$ hybrid on carbon (which is a mixture of 0.00% *s*, 99.97% *p*, and 0.03% *d* atomic). The natural population analysis showed that 173 electrons in the 18-crown-6 (title molecule) are distributed on the sub shells as total-Lewis (core and valence Lewis) and total non-Lewis (valence non-Lewis and Rydberg non-Lewis). The computed values and percentage of each are find below:

Core	53.98724 (99.976% of 54)
Valence Lewis	117.49786 (98.737% of 119)
Total Lewis	171.4851 (99.357% of 173)
Valence non-Lewis	1.15928 (0.6705% of 173)
Rydberg non-Lewis	0.35562 (0.206% of 173)
Total non-Lewis	1.5149 (0.876% of 173)

Global reactivity descriptors

The frontier molecular orbital (FMO) energies of the title molecule were calculated using B3LYP/6-311G (d,p). HOMO energy characterizes the electron giving ability, while LUMO energy characterizes the electron withdrawing ability. Energy gap between HOMO and LUMO characterizes the molecular chemical stability and it is a critical parameter in determining molecular electrical transport properties because it is a measure of electron conductivity. From Fig. 11 and Table 8, HOMO energy is calculated as -7.3709 eV and LUMO energy is calculated as -2.2984 eV by using B3LYP/6-311G (d,p) level. The small energy gap between HOMO and LUMO indicated that charge transfer occurs within the title molecule and the molecule can be easily polarized. Using HOMO and LUMO energies ionization potential and electron affinity can be explicated as $IP \approx -E_{HOMO}$, $EA \approx -E_{LUMO}$. The variation of electro negativity (χ) values is supported by the electrostatic potential. For any two molecules, electron will be partially transferred from one of low χ to that of high χ (electron flow from high

Table 5: Selected experimental and theoretical bond lengths, bond angles and dihedral angles for 18-Crown-6 at the B3LYP/6-311G (d,P) level of theory.

Bond lengths (Å)	18-Crown-6	X-ray [45]	Bond angle (°)	18-Crown-6	X-ray [45]	Dihedral angles (°)	18-Crown-6	X-ray [45]
$C_1 - C_8$	1.513	1.487	$<C_6O_9C_5$	113.303	113.503	$O_{11}C_1C_8O_{12}$	-63.478	-66.478
$C_1 - O_{11}$	1.413	1.422	$<C_2O_{11}C_3$	110.826	112.826	$O_{11}C_1C_8H_{21}$	46.001	62.801
$C_1 - H_{23}$	1.103	1.105	$<C_3O_{10}C_4$	110.826	116.926	$O_{11}C_1C_8H_{22}$	167.368	172.003
$C_1 - H_{24}$	1.099	1.091	$<C_1O_{11}C_8$	109.070	108.270	$H_{23}C_1C_8O_{12}$	56.262	63.062
$C_2 - C_3$	1.513	1.487	$<O_{11}C_1H_{23}$	110.826	110.826	$H_{23}C_1C_8H_{21}$	176.504	176.204
$C_2 - O_{11}$	1.413	1.422	$<C_1H_{23}H_{24}$	108.044	107.544	$H_{23}C_1C_8O_{12}$	-74.888	-66.488
$C_2 - H_{25}$	1.099	1.091	$<C_2H_{25}H_{26}$	108.044	108.244	$C_8C_1O_{11}C_2$	167.368	175.368
$C_2 - H_{26}$	1.103	1.105	$<C_5H_{15}H_{16}$	109.375	109.775	$H_{23}C_1O_{11}C_2$	42.311	62.011
$C_3 - O_{10}$	1.413	1.422	$<O_{11}C_2H_{25}$	108.044	107.644	$H_{24}C_1O_{11}C_2$	-74.888	-66.088
$C_3 - H_{27}$	1.099	1.091	$<C_2C_3H_{27}$	110.439	110.439	$H_{27}C_3O_{10}C_4$	42.001	62.101
$C_3 - H_{28}$	1.103	1.105	$<C_3O_{10}C_4$	113.303	113.303	$H_{28}C_3O_{10}C_4$	-74.888	-66.888
$C_4 - O_{10}$	1.413	1.422	$<C_1O_{11}C_2$	113.303	117.303	$C_7C_6O_9C_5$	176.504	176.504
$C_4 - H_{13}$	1.103	1.105	$<C_7O_{12}C_8$	113.303	115.603	$C_1O_{13}C_{12}H_{41}$	-63.478	-63.062
$C_5 - O_9$	1.423	1.422	$<C_{12}H_{41}H_{42}$	108.044	107.544	$H_{32}C_5C_6H_{30}$	167.368	175.368
$C_5 - H_{16}$	1.099	1.091	$<O_{17}C_4H_{34}$	110.826	109.526	$O_{18}C_3C_4H_{34}$	46.001	-2.444
$C_6 - C_7$	1.513	1.487				Net charges		
$C_6 - H_{17}$	1.103	1.105				O_1	-0.356	
$C_6 - H_{18}$	1.099	1.091				O_2	-0.356	
$C_8 - O_{12}$	1.423	1.422				O_3	-0.359	
$C_4 - O_{10}$	1.423	1.422				O_4	-0.360	
$C_7 - C_{27}$	1.513	1.487				O_5	-0.360	
$C_8 - O_{15}$	1.413	1.422				O_6	-0.468	
$C_8 - H_{25}$	1.099	1.091				Cu	0.065	
$C_8 - H_{26}$	1.103	1.105						
$C_9 - C_{10}$	1.513	1.487						
$C_9 - O_{15}$	1.413	1.422						
$C_9 - H_{23}$	1.099	1.091						
$C_8 - H_{26}$	1.103	1.105						
$C_{10} - O_{14}$	1.413	1.422						
$C_{10} - H_{21}$	1.103	1.105						
$C_{10} - H_{22}$	1.099	1.091						
$C_{11} - C_{12}$	1.513	1.487						
$C_{11} - O_{14}$	1.413	1.422						
$C_{12} - H_{41}$	1.103	1.105						
$C_{12} - H_{42}$	1.099	1.091						
$C_{12} - C_{13}$	1.513	1.487						

Table 6: Second Order Perturbation Theory Analysis of Fock Matrix in NBO Basis for 18-Crown-6 by B3LYP/6-311G (d,p).

Donor 18-Crown-6	Type	ED(i)(e)	Acceptor	Type	ED(i)(e)	$E^{(2)a}$(kcal/mol)	E(j)-E(i)[b](a.u)	F(ij)[c](a.u)
BDC2-H38	σ	0.99192	BD*C1 - O13	σ *	0.01131	1.74	0.82	0.048
BDC3-H36	σ	0.99162	BD*C4 - O17	σ *	0.01070	1.90	0.83	0.050
BDC4-H33	σ	0.99186	BD*C3 - O18	σ *	0.01069	1.83	0.83	0.049
BDC12-H42	σ	0.99160	BD*C11 -O14	σ *	0.02213	1.72	0.80	0.047
LP(2)O13		0.95903	BD*C1 - H39	σ *	0.01384	3.21	0.68	0.060
LP(2)O13		0.95903	BD*C12-H42	σ *	0.01656	4.36	0.67	0.069
LP(2)O14		0.96592	BD*C10-H21	σ *	0.01186	2.95	0.70	0.058
LP(2)O14		0.96592	BD*C11-H19	σ *	0.01186	2.96	0.70	0.058
LP(2)O15		0.95904	BD*C9-H24	σ *	0.01655	4.36	0.67	0.069
LP(2)O16		0.95778	BD*C6-H30	σ *	0.01529	3.66	0.68	0.064
LP(2)O16		0.95778	BD*C7-H27	σ *	0.01441	3.99	0.67	0.066
LP(2)O17		0.95727	BD*C4-H33	σ *	0.01463	3.97	0.67	0.066
LP(2)O17		0.95727	BD*C5-H32	σ *	0.01481	2.76	0.68	0.055
LP(2)O18		0.95779	BD*C2-H37	σ *	0.01473	2.73	0.68	0.055

[a] *$E^{(2)}$ means energy of hyperconjugative interactions (stabilization energy).*
[b] *Energy difference between donor and acceptor i and j NBO orbitals.*
[c] *$F_{(i,j)}$ is the Fock matrix element between i and j NBO orbital.*
$LP_{(n)}$ is a valence lone pair orbital (n) on atom.

Table 7: Occupancy of natural orbitals (NBOs) and hybrids of 18-Crown-6 by /6- B3LYP 311G (d,p).

Donor Lewis-type (NBOs) 18-Crown-4	Occupancy	Hybrid	AO [%]
σ BDC2-H38	0.99192	$sp^{3.23}$	s(23.63%)p(76.29%)d(0.08%)
σ BDC3-H36	0.99162	$sp^{3.25}$	s(23.52%)p(76.40%)d(0.08%)
σ BDC4-H33	0.99186	$sp^{3.23}$	s(23.65%)p(76.28%)d(0.08%)
σ BDC12-H42	0.99160	$sp^{3.13}$	s(24.20%)p(75.73%)d(0.07%)
LP(2)O13	0.95903	$p^{99.99}$	s(0.02%)p(99.94%)d(0.04%)
LP(2)O14	0.96592	$p^{1.00}$	s(0.00%)p(99.97%)d(0.03%)
LP(2)O15	0.95904	$p^{99.99}$	s(0.02%)p(99.94%)d(0.04%)
LP(2)O16	0.95778	$p^{1.00}$	s(0.01%)p(99.95%)d(0.04%)
LP(2)O17	0.95727	$p^{1.00}$	s(0.00%)p(99.96%)d(0.04%)
LP(2)O18	0.95779	$p^{1.00}$	s(0.01%)p(99.95%)d(0.04%)

Table 8: The ionisation potential (I /eV), electron affinity (A /eV), chemical hardness (η/ eV), softness (S/ eV^{-1}), chemical potential (μ), electronegativity (χ/eV), and electrophilicity (ω/ eV) of 18-Crown-6 using B3LYP/6-311G (d,P).

Compounds	I (eV)	A(eV)	*X*(eV)	*μ* (eV)	η (eV)	*S*(eV^{-1})	ω (eV)
18-Crown-6	7.3709	2.2984	4.8347	-4.8347	2.5363	0.1971	4.6079

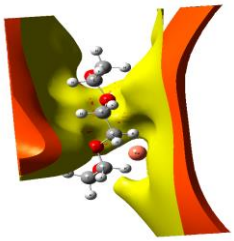

ESP

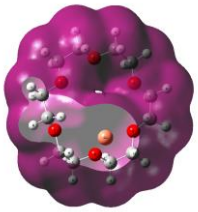

Total density

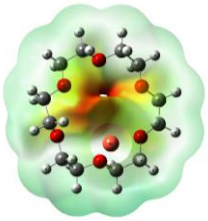

MEP

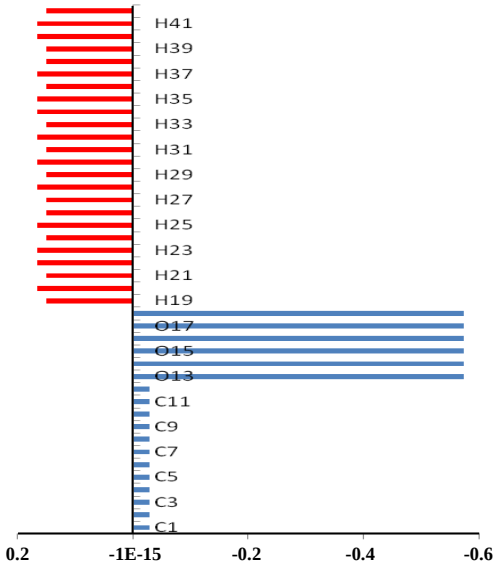

Fig. 11: Molecular surfaces and atomic charge distribution (au) of the 18-crown-6 using B3LYP/6-311G (d,p).

chemical potential to low chemical potential). The chemical hardness (η) = ($IP - EA$)/2, electro negativity (χ) = ($IP + EA$)/2, chemical potential (μ) = - ($IP + EA$)/2, ω = μ^2/ 2η (electrophilicity), and chemical softness (S) = 1/2η, values were calculated as 2.536, 4.835, -4.835, 4.608 and 0.197 respectively. Obtained small η value means that the charge transfer occurs in the molecule. Considering the η values, large HOMO – LUMO gap means a hard molecule and small HOMO – LUMO gap means a soft molecule. Additionally, it can be said that the small HOMO – LUMO energy gap represents more reactive molecule.

Natural charge and exact configuration

The natural population analysis performed on the electronic structures of the title molecule clearly describes the distribution of electrons in various sub-shells of their atomic orbits. The accumulation of charges on the individual atom and the accumulation of electrons in the core, valence and Rydberg sub-shells and natural electronic configuration are also presented in Table 9. In our title molecule, the most electronegative center charge of −0.6262, −0.5812, −0.5810, −0.5722 −0.5718, and −0.5718 are accumulated on O_{14}, O_{15}, O_{13}, O_{17}, O_{16}, and O_{18}-atoms. According to an electrostatic point of view of the molecule, these electronegative atoms have a tendency to donate electrons. Also, it is found that the most electropositive center charge of 0.17748, 0.17236, 0.16478, 0.16413 and 0.16359 are accumulated on H_{22}, H_{40}, H_{37}, H_{35}, and H_{32}-atoms. According to an electrostatic point of view of the molecule, these electropositive atoms have a tendency to accept electrons. The natural electronic configuration of each electronegative and electropositive atom is listed in Table 9.

Other molecular properties

The 3D plots of Highest Occupied Molecular Orbital (HOMO) and the Lowest Unoccupied Molecular Orbital (LUMO), ElectroStatic Potential (ESP), Electron Density (ED), and the Molecular Electrostatic Potential (MEP) map for the title molecule at the B3LYP method

Table 9: Natural Charge, Natural Population and Natural electronic Configuration of 18-Crown-6 using B3LYP/6-311G (d,P).

Compound	Atom No.	Natural Charge	Natural Population				Natural electronic Configuration
18-Crown-6			Core	Valence	Rydberg	total	
	C1	-0.0361	1.999	4.01639	0.0206	6.036	[core]2S(1.00)2p(3.01)3S(0.01)3p(0.01)3d(0.01)
	C2	-0.0302	1.999	4.0111	0.01996	6.030	[core]2S(1.00)2p(3.01)3S(0.01)3p(0.01)3d(0.01)
	C3	-0.0284	1.999	4.00949	0.01978	6.028	[core]2S(1.00)2p(3.01)3S(0.01)3p(0.01)3d(0.01)
	C4	-0.0281	1.999	4.00896	0.01998	6.028	[core]2S(1.00)2p(3.01)3S(0.01)3p(0.01)3d(0.01)
	C5	-0.0281	1.999	4.00895	0.01998	6.028	[core]2S(1.00)2p(3.01)3S(0.01)3p(0.01)3d(0.01)
	C6	-0.0284	1.999	4.00948	0.01978	6.028	[core]2S(1.00)2p(3.01)3S(0.01)3p(0.01)3d(0.01)
	C7	-0.0302	1.999	4.0111	0.01996	6.030	[core]2S(1.00)2p(3.01)3S(0.01)3p(0.01)3d(0.01)
	C8	-0.0361	1.999	4.01641	0.02061	6.036	[core]2S(1.00)2p(3.01)3S(0.01)3p(0.01)3d(0.01)
	C9	-0.0522	1.999	4.02773	0.02533	6.052	[core]2S(1.00)2p(3.03)3S(0.01)3p(0.01)3d(0.01)
	C10	-0.0278	1.999	4.00822	0.02041	6.027	[core]2S(1.01)2p(3.00)3S(0.01)3p(0.01)3d(0.01)
	C11	-0.0278	1.999	4.00821	0.02042	6.027	[core]2S(1.01)2p(3.00)3S(0.01)3p(0.01)3d(0.01)
	C12	-0.0522	1.999	4.02774	0.02534	6.052	[core]2S(1.00)2p(3.03)3S(0.01)3p(0.01)3d(0.01)
	O13	-0.5810	1.999	6.56835	0.01295	8.581	[core]2S(1.62)2p(4.94)3p(0.01)
	O14	-0.6262	1.999	6.60931	0.01719	8.626	[core]2S(1.62)2p(4.99)3p(0.01)
	O15	-0.5812	1.999	6.56837	0.01295	8.581	[core]2S(1.62)2p(4.94)3p(0.01)
	O16	-0.5718	1.999	6.55925	0.01281	8.571	[core]2S(1.62)2p(4.94)3p(0.01)
	O17	-0.5722	1.999	6.55983	0.01261	8.572	[core]2S(1.62)2p(4.94)3p(0.01)
	O18	-0.5718	1.999	6.5593	0.01281	8.571	[core]2S(1.62)2p(4.94)3p(0.01)
	H19	0.1617	0	0.83338	0.00492	0.838	1S(0.83)
	H20	0.17743	0	0.81645	0.00613	0.822	1S(0.82)2S(0.01)
	H21	0.16168	0	0.83339	0.00492	0.838	1S(0.83)
	H22	0.17748	0	0.81639	0.00613	0.822	1S(0.82)2S(0.01)
	H23	0.15844	0	0.82922	0.01234	0.841	1S(0.83)2S(0.01)
	H24	0.16054	0	0.83481	0.00465	0.839	1S(0.83)
	H25	0.17232	0	0.81765	0.01002	0.827	1S(0.82)2S(0.01)
	H26	0.15177	0	0.84305	0.00518	0.848	1S(0.84)

Table 9: Natural Charge, Natural Population and Natural electronic Configuration of 18-Crown-6 using B3LYP/6-311G (d,P). (Continued)

Compound	Atom No.	Natural Charge	Natural Population				Natural electronic Configuration
18-Crown-6			Core	Valence	Rydberg	total	
	H27	0.15191	0	0.84317	0.00492	0.848	1S(0.84)
	H28	0.16477	0	0.82926	0.00597	0.835	1S(0.83)2S(0.01)
	H29	0.1511	0	0.84399	0.00491	0.848	1S(0.84)
	H30	0.16408	0	0.8302	0.00572	0.835	1S(0.83)
	H31	0.15094	0	0.84414	0.00492	0.849	1S(0.84)
	H32	0.16359	0	0.83058	0.00584	0.836	1S(0.83)
	H33	0.15095	0	0.84413	0.00492	0.849	1S(0.84)
	H34	0.16359	0	0.83057	0.00584	0.836	1S(0.83)
	H35	0.16413	0	0.83015	0.00572	0.835	1S(0.83)
	H36	0.15109	0	0.84399	0.00491	0.848	1S(0.84)
	H37	0.16478	0	0.82924	0.00597	0.835	1S(0.83)2S(0.01)
	H38	0.15192	0	0.84317	0.00491	0.848	1S(0.84)
	H39	0.15176	0	0.84306	0.00518	0.848	1S(0.84)
	H40	0.17236	0	0.81764	0.01	0.827	1S(0.82)2S(0.01)
	H41	0.15839	0	0.82928	0.01234	0.841	1S(0.83)2S(0.01)
	H42	0.16054	0	0.83481	0.00465	0.839	1S(0.83)
	Cu43	0.05247	17.99	10.9420	0.0063	28.94	[core]4S(1.23)3d(9.71)5S(0.01)

Core	53.98724 (99.976% of 54)
Valence Lewis	117.49786 (98.737% of 119)
==========	==========
Total Lewis	171.4851 (99.357% of 173)

Valence non-Lewis	1.15928 (0.6705% of 173)
Rydberg non-Lewis	0.35562 (0.206% of 173)
==========	==========
Total non-Lewis	1.5149 (0.876% of 173)

with 6-311G (d,p) level are shown in Figs. (10 and 11). The ED plot for the title molecule shows a uniform distribution. While the negative ESP is localized more over the oxygen atoms, the positive ESP is localized on the rest of the title molecule.

MEP has been used primarily for predicting sites and relative reactivity's towards electrophilic and nucleophilic attack, and in studies of biological recognition and hydrogen bonding interactions [50-52]. The calculated 3D MEP of the title compound was calculated from optimized molecular structure by using B3LYP/6–311G (d,p) level and also shown in Fig. 11. The color scheme for the MEP surface is as follows: red for electron rich, partially negative charge; blue for electron deficient, partially positive charge; light blue for slightly electron deficient region; yellow for slightly electron rich region; green for neutral (zero potential); respectively [40]. According to our results, the negative region (red) is mainly over the O atomic sites, which were caused by the contribution of lone-pair electrons of oxygen atom while the positive (blue) potential sites are around the hydrogen and carbon atoms. A portion of a molecule that has a negative electrostatic potential will be susceptible to electrophilic attack—the more negative is the better. It is not as straightforward to use electrostatic potentials to predict nucleophilic attack [53]. Hence, the negative region (red) and positive region (blue) indicate electrophilic and nucleophilic attack symptoms. Also,

Table 10: Total static dipol moment (μ), the mean polarizability (<α>), the anisotropy of the polarizability (Δα), the mean first-order hyperpolarizability (<β>) and third-order hyperpolarizability (<γ>) for 18-Crown-6 using B3LYP/6-311G (d,P).

Property	PNA	B3LYP/6-311G(d,P) 18-Crown-6
μ_x		-0.2455Debye
μ_y		0.0009Debye
μ_z		-0.4252Debye
μ	2.44 Debye [a]	0.49096 Debye
α_{XX}		201.47005 a.u.
α_{XY}		-0.0433389 a.u.
α_{YY}		225.11336 a.u.
α_{ZZ}		10.387977 a.u.
α_{YZ}		0.0114888 a.u.
α_{XZ}		154.005473 a.u.
< α>	22×10^{-24} cm[3b]	28.68×10^{-24} esu
Δα		9.67×10^{-24} esu
βxxx		-28.7088 a.u.
βxxy		0.0057 a.u.
βxyy		-5.2599 a.u.
βyyy		-0.0135 a.u.
βxxz		-8.1370 a.u.
βxyz		-0.0546 a.u.
βyyz		13.3664 a.u.
βxzz		-13.0446 a.u.
βyzz		0.0039 a.u.
βzzz		18.8159 a.u.
< β>	15.5×10^{-30} esu[c]	29.65×10^{-30} esu
γxxxx		-4319.2002 a.u.
γyyyy		-3847.7809 a.u.
γzzzz		-614.1769 a.u.
γxxyy		-1345.0567 a.u.
γxxzz		-882.8252 a.u.
γyyzz		-798.0568 a.u.
⟨γ⟩		25.63×10^{-30} esu

a, b, c) PNA results are taken from references [63-65].

Table 11: Theoretical UV spectra of 18-Crown-6, calculated at CAM-B3LYP/6–311G (d, p).

TD-Theoretical												
Gas phase					water				ethanol			
state	Configuration	Coeffic ient	f	λ, nm	Config uration	Coeffic ient	f	λ, nm	Configuration	Coeffici ent	f	λ, nm
I	87-> 88 87->91 87-> 9 87->99 86->89	0.91 -0.2 0. 26 0.16 0.14	0.12	316	87-> 88 87->91 87->94 87->96 87->99 86->88	0.94 0.15 0.15 -0.1 -0.2 0.13	0.16	295	-87> 88 - 87>91 -87>94 -87>95 -87>99 -86>88	0.93 0.16 0.14 0. 14 -0.2 0.13	0.17	298
II	87-> 88 87->91 -87> 95 86->89 86->91 86->95 86->99	-0.3 -0.1 0. 20 0.79 0.24 0.31 -0.2	0.06	240	87-> 89 87->90 87->95 87->98 87->100 87-104	0.50 -0.4 0.59 -0.3 -0.2 -0.2	0.13	234	87-> 89 87->90 87->96 87->98 87-100 87-103 87-104	0.52 -0.4 0.59 -0. 3 0.2- -0.1 -0.2	0.13	235
III	-87> 88 -87>94 -87>95 -87>99 -86>89	0.2- 0.56 0. 72 0.14 -0.2	0.05	229	-87> 88 -86>88 -86>91 -86>94 -86>95 -86>99	-0.2 0.88 -0.2 -0.1 -0.2 0.22	0.11	228	87-> 88 86->88 86->91 86->94 86->95 86->99	-0.2 0.88 0.2- -0.1 0.2- 0.22	0.11	229
IV	87-> 90 87->92 87-> 93 87->96 87->98 87->100 87->103 87->104 87->108	0.51 0.40 0.1- 0.46 0.41 0. 1- 0.17 0.26 0.13	0.05	220	87-> 89 87->90 87->92 87->93 87->97 87->98 87-100 87-101	0.33 0.11 0.60 0.19 -0.43 0.47 -0.13 -0.17	0.04	225	87-> 89 87->92 87->93 87->97 87->98 87-100 87-101	0.32 0.61 0.18 -0.4 0.51 -0.1 -0.2	0.04	227

a negative electrostatic potential region is observed around the O atom.

The corresponding Mulliken's plot with B3LYP/6-311G (d,p) method are shown in Fig. 11. It is noted that from Fig. 11, the strong negative and positive partial charges on the skeletal atoms (especially O_{13}, O_{14}, C_1, C_2, O_{15}, O_{16}, O_{17}, O_{18}, C_3, C_4, C_5, C_6, C_7, C_8, H_{17}, H_{18}, H_{24}, H_{25}) for the selected compounds increase with increasing Hammett constant of substituent groups [54, 55]. These distributions of partial charges on the skeletal atoms show that the electrostatic repulsion or attraction between atoms can give a significant contribution to the intra- and intermolecular interaction.

Nonlinear optical (NLO) Analysis

P-nitroaniline (PNA) is one of the prototypical molecules used in the study of the NLO properties of molecular systems. In this study, the typical NLO material, PNA was chosen as a reference molecule; because there were no experimental values about the title compound in the literature. The relatively NLO of the title molecule compared to PNA indicate their promising applications in NLO materials. Therefore it was used frequently as a threshold value for comparative purposes and still continues to be a recognized prototype of organic NLO chromophores. Its hyperpolarizability was studied both experimentally and theoretically in various solvents and at different frequencies [56-59].

Polarizabilities and hyperpolarizabilities characterize the response of a system in an applied electric field [60]. They determine not only the strength of molecular interactions as well as the cross-sections of different scattering and collision processes, but also the non-linear optical (NLO) properties of the system [61, 62]. In order to investigate the relationships among photocurrent generation, molecular structures and NLO, the polarizabilities and hyperpolarizabilities of title compound was calculated using B3LYP method, 6-311G (d,p) basis set, based on the finite-field approach. The mean first order hyperpolarizability $\langle\beta\rangle$, third-order

hyperpolarizability ⟨γ⟩, total static dipole moment (μ), the mean polarizability (<α>), and the anisotropy of the polarizability (Δα), of title molecule are presented in Table 10. The calculated value of dipole moment was found to be 0.49096 D at B3LYP/6-311G (d,p). The calculated mean polarizability (<α>) is $28.68x10^{-24}$esu i.e. higher than PNA molecule. In addition, the calculated mean first order hyperpolarizability⟨β⟩, of the title molecule is $29.65x10^{-30}$ esu and third-order hyperpolarizability ⟨γ⟩, is $25.63x10^{-30}$ i.e. higher than PNA molecule [63-65]. This result indicates the linearity of the title molecule and promising the title molecule to be used as NLO materials.

Electronic absorption spectra of the title compound 18-crown-6

The electronic spectra of compound 18-crown-6 in ethanol and water solvents and the assignment of spectra are given in Fig. 12 and Table 11. The charge density maps of the occupied and vacant MO·s considered in the transitions is presented in Fig. 13. The spectrum in ethanol and water is composed of four bands centered at 298, 295 nm, 235, 234 nm, 229, 228 nm, and 227, 225 nm. All bands are assigned to (π-π*) transitions as reflected from their intensities (0-30,000). The excited configurations considered in compound 18-crown-6 are those which results from an electron excitation of two highest occupied molecular orbital's φ_{86}, φ_{87} and the lowest seven vacant molecular orbital's φ_{88}, φ_{89}, φ_{91}, $\varphi_{94}{}^{-1}\varphi_{96}$, φ_{99} .

The first $(\pi\text{-}\pi^*)^1$ state is centered at 298, 295 nm in ethanol and water this band is predicted theoretically gas phase at 316 nm, and is composed of a mixture of six configurations, (c.f. Table 11) and assigned as CT, localized and delocalized configurations may be expected. The second $(\pi\text{-}\pi^*)^1$ state is centered at 235, 234 nm in ethanol and water and is predicted theoretically gas phase at 240 nm. This state is composed of a mixture of seven configurations, namely, $\varphi_{87}{}^{-1}\varphi_{88}$, $\varphi_{87}{}^{-1}\varphi_{91}$, $\varphi_{87}{}^{-1}\varphi_{95}$, $\varphi_{86}{}^{-1}\varphi_{89}$, $\varphi_{86}{}^{-1}\varphi_{91}$, $\varphi_{86}{}^{-1}\varphi_{95}$ and $\varphi_{86}{}^{-1}\varphi_{99}$, that is, delocalized configurations and CT character may be expected (Fig. 13). The third $(\pi\text{-}\pi^*)^1$ state is centered in ethanol and water at 229, 228 nm and predicted theoretically gas phase at 229 nm. This band is composed of a mixture of six configurations, (Table 11) and assigned as CT character

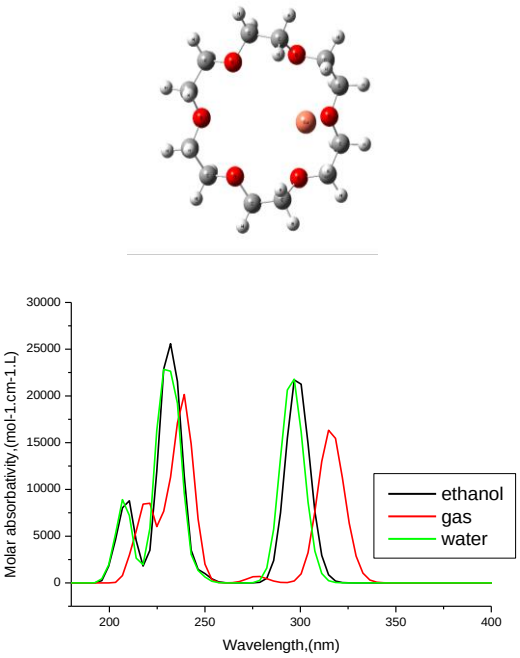

Fig. 12: Electronic absorption spectra of compound (18-crown-6).

and delocalized band. The main contribution of this band is coming from the one configuration $\varphi^{-1}{}_{86}$ φ_{88}, which is of CT character may be expected (Fig. 13). The fourth $(\pi, \pi^*)^1$ state computed at 227, 225 nm in ethanol and water, and is computed theoretically gas phase at 220 nm. This state is composed of a mixture of nine configurations, which is also assigned as a delocalized, localized, and a charge transfer band (CT) (Fig. 13).

CONCLUSIONS

The molecular geometry of compound 18-crown-6 in the ground state has been calculated by using density function theory (DFT-B3LYP/6-311G (d,p) level of theory. The optimized structure of the molecule is non-planar as indicated from the dihedral angles. The HOMO-LUMO energy gap helped in analyzing the chemical reactivity, hardness, softness, chemical potential and electronegativity. Mullikan and natural charge distribution of the molecule 18-crown-6 were studied which indicated the electronic charge distribution in the molecule 18-crown-6. The calculated dipole moment and first order hyperpolarizability results indicate that the molecule 18-crown-6 has a reasonable good linear optical

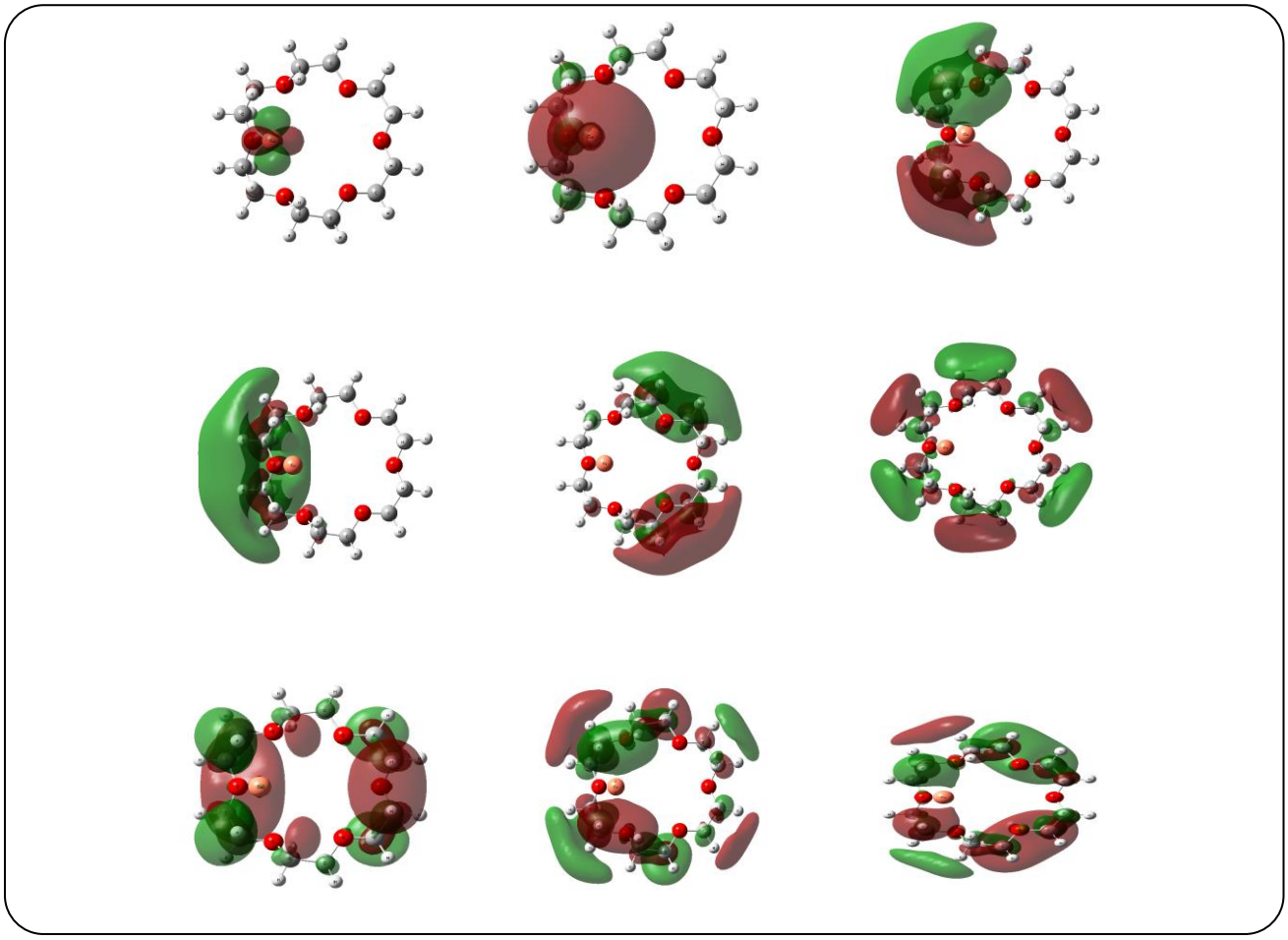

Fig. 13: The charge density maps of the occupied and unoccupied MO's for compound 18-crown-6.

behavior. The NBO analysis indicated the intermolecular charge transfer between the bonding and anti-bonding orbital's. MEP confirmed the different negative and positive potential sites of the molecule in accordance with the total electron density surface. All bands in the UV spectra can be assigned to (π-π*) transitions as reflected from their intensities. The solvent dependence of the bands can be attributed to the change in the transition dipole moments of the ground and excited states. According to the high activity in physical parameters of 18-crown-6 E_{HOMO}, E_{LUMO}, E_{gap} and dipole moment (μ) was applied for the interaction with nano $CuSO_4$ solutions in 10% ethanol –water solvents form 1:1 and 1:2 M/L complexes with increasing of the thermodynamic parameters, Gibbs free energies, enthalpies and entropies of solvation by increasing of temperature indicating more interactions.

Received : Jul. 9, 2018 ; Accepted : Nov. 14, 2018

REFERENCES

[1] Pedersen C.J., Crystalline Salt Complexes of Macrocyclic Polyether's, *J. Am. Chem. Soc.* **89**: 385-391 7017 (1967).

[2] Arnaud-Neu F., Delgado R., Chaves S., Critical Evaluation of Stability Constants and Thermodynamic Functions of Metal Complexes of Crown Ethers, *Pure. Appl. Chem.* **75**: 71-102 (2003).

[3] Wong P.S.H., Antonio B.J., Dearden D.V., Gas-Phase Studies of Valinomycin-Alkali Metal Cation Complexes: Attachment Rates and Cation Affinities' *J. Am. Soc. Mass Spectrosc*. **5**: 632-637 (1994).

[4] Tsatsas A.T., Stearns R.W., Risen W.M., Nature of alkali metal Ion Interactions with Cyclic Polyfunctional Molecules. I. Vibrations of Alkali Ions Encaged by Crown Ethers in Solution, *J. Am. Chem. Soc.* **94**: 5247-5253 (1972).

[5] Popov A.I., Lehn J.M., in: G.A., Melson (Ed.), "Coordination Chemistry of Macrocyclic Compounds", Plenum, New York, **537**: (1979), Lamb J.D., Izatt R.M., Christensen J.J., Eatough D.J., in: Melson G.A. (Ed.), "Coordination Chemistry of Macrocyclic Compounds", Plenum, New York, **145**: (1979).

[6] Hay B.P., Rustad J.R., Zipperer J.P., Wester D.W., Topological Electron Density Analysis of Organosulfur Compounds, *J. Mol. Struct.* **337**: 201-207 (1995).

[7] El-Azhary A.A., Al-Kahtani A. A., Conformational Study of the Structure of Free 12-Crown-4, *J. Phys. Chem.* A **108**: 9601-9607 (2004).

[8] El-Azhary A A, Al-Kahtani A A, Experimental and Theoretical Study of the Vibrational Spectra of Free 12-Crown-4, *J. Phys. Chem.* A, **109**: 4505-4511 (2005).

[9] Hori K.N., Dou K., Okano A., Ohgami, Tsukube H., Stable of 12-crown-O$_3$N and its Li$^+$ Complex in Aqueous Solution, *J. Comp. Chem.*, **23**: 1226-1235 (2002).

[10] Onsager L., Electric Moments of Molecules in Liquids, *J. Am. Chem. Soc.*, **58**: 1486-1493 (1936).

[11] Cramer C.J., Truhlar D.G., Implicit Solvation Models: Equilibria, Structure, Spectra, and Dynamics, *Chem. Rev.*, **99**: 2161-2200 (1999).

[12] Tanika Arora, Hashim Ali, William A. Burns, Eiko Koizumi, Hideya Koizumi, Theoretical and ATR-FTIR Study of Free 12-Crown-4 in Aqueous Solution, *Chem. Phys. Letts.*, **502**: 253-258 (2011).

[13] Mandal K., Kar T., Nandi P.K., Bhattacharyya S.P., Theoretical Study of the Nonlinear Polarizabilities in H_2N and NO_2 Substituted Chromophores Containing Two Hetero Aromatic Rings, *Chem. Phys. Letts.*,**376**: 116-124 (2003).

[14] Nandi P.K, Mandal K., Kar T., Effect of Structural Changes in Sesquifulvalene on the Intramolecular Charge Transfer and Nonlinear Polarizations – A Theoretical Study, *Chem. Phys. Letts.*, **381**: 230-238 (2003).

[15] Prasad P.N., Williams D.J., "Introduction to Nonlinear Optical Effects in Molecules and Polymers", John Wiley & Sons, Inc., New York, NY, USA. (1991).

[16] Meyers F., Marder S.R., Pierce B.M., Brédas J.L., Electric Field Modulated Nonlinear Optical Properties of Donor-Acceptor Polyenes: Sum-Over-States Investigation of the Relationship between Molecular Polarizabilities (.Alpha., .Beta., and Gamma.) and Bond Length Alternation, *J. Am. Chem. Soc.*, **116**: 10703- 10714 (1994).

[17] Foster J.P., Weinhold F., Natural Hybrid Orbitals, *J. Am. Chem. Soc* **102**: 7211-7218 (1980).

[18] Reed A.E., Curtiss L.A., Weinhold F., Intermolecular Interactions from a Natural Bond Orbital, Donor-Acceptor Viewpoint, *Chem. Rev.*, **88**: 899-926 (1988).

[19] Holleman A.F., Wiberg E., "Inor. Chem.", San Diego: Acad. Press. ISBN 0-12-352651-5 (2001).

[20] David A., Wright and Pamela Welbourn Environmental Toxicology, *Cambridge University Press, UK.* (2002).

[21] El Sayed M, Abou Elleef, Esam A Gomaa, Thermodynamics of Salvations for Nano Zinc Oxide in 2 MNH_4Cl+ Mixed DMF – H_2O Solvents at Different Temperatures, *International Journal of Engineering and Innovative Technology*, **2**: 121-126 (2013).

[22] Esam A, Gomaa, Ame. Thermodynamics of Complex Formation (Conductometrically) between Cu (II) Ion and 4-Phenyl -1- Diacetyl Monoxime –3 -Thiosemicarbazone (BMPTS) In Methanol at Different Temperatures, *J. Sys. Sci.* **3**: 12-25 (2014).

[23] (a) Becke A., Densityfunctional Thermochemistry III. the Role of Exact Exchange, *Chem. Phys.*, **98**: 5648-5652 (1993)

(b) Becke A., Densityfunctional Thermochemistry III. the Role of Exact Exchange, *Chem. Phys.*, **98**: 1372-1376 (1993).

[24] Lee C., Yang W., Parr R.G., Development of the Colle-Salvetti Correlation-Energy Formula Into a Functional at the Electron Density, *Phys. Rev. B Condens. Matter.***157:** 785-789 (1988).

[25] Stefanov B., Liu B.G., Liashenko A., Piskorz P., Komaromi I., Martin R.L., Fox D.J., Keith T., Al-Laham M.A., Peng C.Y., Nanayakkara A., Challacombe M, Gill P.M., W, Johnson B., Chen W., Wong M.W. , Gonzalez C., Pople J.A., Gaussian, Inc., Pittsburgh PA, (2003).

[26] Frisch M., Trucks J.G.W, Schlegel H.B, Scuseria G.E., et al, Gaussian, Inc., Wallingford CT. (2009).

[27] Dennington, Keith R., Millam T., Semichem J., Gaussview, Version 5 Inc., Shawnee Mission KS. (2009).

[28] Avci D., Second and Third-Order Nonlinear Optical Properties and Molecular Parameters of Azo Chromophores: Semiempirical Analysis, *Spectrochimica Acta A.*, **82**: 37- 43 (2011).

[29] Avci D., Başoğlu A., Atalay Y., NLO and NBO Analysis of Sarcosine Maleic Acid by Using HF and B3LYP Calculations, *Struct. Chem.*, **21**: 213-219 (2010).

[30] Avci D., Cömert H., Atalay Y., Ab Initio Hartree-Fock Calculations on Linear and Second-Order Nonlinear Optical Properties of New Acridine-Benzothiazolylamine Chromophores, *J. Mol. Modeling*, **14**: 161-171 (2008).

[31] Pearson R.G., Absolute Electro Negativity and Hardness Correlated with Molecular Orbital Theory, *Proc. Nat. Acad. Sci.* **83**: 8440-8441 (1986).

[32] Chandra A.K., Uchimara T., NLO and NBO Analysis of Sarcosine-Maleic Acid by Using HF and B3LYP Calculations, *J. Phy. Chem. A*, **105**: 3578-3582 (2001).

[33] Chocholoušová J., Špirko V., Hobza P., First Local Minimum of the Formic Acid Dimer Exhibits Simultaneously Red-Shifted O–H-O and Improper Blue-Shifted C–H…O Hydrogen Bonds, *Phys. Chem.*, **6**: 37- 41 (2004).

[34] Szafran M., Komasa A., Bartoszak-Adamska E., Crystal and Molecular Sructure of 4-Carboxypiperidinium Chloride (4-Piperidinecarboxylic Acid Hydrochloride), *J. Mol. Struct.* **827**: 101-107 (2007).

[35] Ives D.J.G., Chemical Thermodynamics, *University Chemistry, Maconald Technical and Scientific.* (1971).

[36] Dickenson R. E., Geis I., "Benjamin Chemistry", Matter W.A., and the Universe, Inc., USA. (1976).

[37] Oswal S.L., Desai J. S., Ijardar S. P., Jain D. M., Studies of Partial Molar Volumes of Alkylamine in Non-Electrolyte Solvents II. Alkyl Amines in Chloroalkanes at 303.15 And 313.15 K., *J. Mol. Liquids.*, **144**: 108-114 (2009).

[38] Zhang D.E., Zhang X.J., Ni X.M., Zheng H.G., Yang D.D., Synthesis and Characterization of $Nife_2o_4$ Magnetic Nanorods *via* A PEG-Assisted Route, *J. Magn. Mater.*, **292**: 79-82 (2005).

[39] Xia B.Y., Yang P.D., Sun Y.G., One-Dimensional Nanostructures: Synthesis, Characterization, and Applications, *Adv Mater* **15**: 353- 356 (2003).

[40] Duan X., Huang Y., Cui Y., Wang J., Lieber C.M., Indium Phosphide Nanowires as Building Blocks for Nanoscale Electronic and Optoelectronic Devices, *Nature* 66-69 (2001)

[41] Mohamed N.H., Hamed Esam A, Gomaa Sameh G, Thermodynamics of Solvation for Nano Zinc Carbonate In Mixed DMF–H2O Solvents at Different Temperatures, *International Journal of Engineering and Innovative Technology (IJEIT)*, **4**: 203-207 (2014).

[42] Liu W.J., He W.D., Zhang Z.C., Nanogenerators-from Scientific Discovery to Future Applications, *J. Cryst Growth* **290**: 592-598 (2006).

[43] Yizahak Marcus, Solubility and Solvation in Mixed Solvent Systems, *Pure and Applied Chem.*, **62**: 2069-2076 (1990).

[44] Chen L., Shen L., Xie A., Zhu J., Wu Z., Yang L., Discovery of Diamond in Eclogite from the Chinese Continental Scientific Drilling Project Main Hole (CCSD-MH) in the Sulu UHPM Belt [In Chinese], *Cryst Res Technol.*, **42**: 886-891 (2007).

[45] Yurii A., Simonov A., Alexandr, Dvorkin, Marina, S, Fonari, Tadeush, I, Malinowski, Elzbieta Luboch, Andrzej Cygan, Jan F, Biernat, V, Edward, Ganin, Popkov, Investigation of Structural, Thermal and Magnetic Behaviors of Pristine Barium Carbonate Nanoparticles Synthesized by Chemical Co-Precipitation Method, *J. Inclusion Phenomena and Molecular Recognition in Chemistry*, **15**: 79-85 (1993).

[46] Snehalatha M., Ravikumar C., Hubert Joe I., Sekar N., Jayakumar V.S., Vibrational Spectra and Scaled Quantum Chemical Studies of the Structure of Martius Yellow Sodium Saltmonohydrate, *Spectrochim. Acta A*, **72**: 1121-1126 (2009).

[47] James C., Amal A., Raj, Reghunathan R., Joe I.H., Jayakumar V.S., Structural Conformation and Vibrational Spectroscopic Studies of 2,6-Bis (P-N, N-Dimethyl Benzylidene) Cyclohexanone Using Density Functional Theory, *J. Raman Spectrosc.*, **37**: 1381-1392 (2006).

[48] Liu J., Chen Z., Yuan S., Zhejiang J., Study on the Prediction of Visible Absorption Maxima of Azobenzene Compounds, *Univ. Sci. B*, **6**: 584-589 (2005).

[49] Rubarani P., Gangadharan S., Krishnan S., Natural Bond Orbital (NBO) Population Analysis of 1-Azanapthalene-8-Ol, *Acta Physica Polonica A.*, **125**: 18-22 (2014).

[50] Scrocco E., Tomasi J., Interpretation by Means of Electrostatic Molecular Potentials, *Advances in Quantum Chemistry*, **11**: (1979) 115-120.

[51] Luque F.J., López J.M., Orozco M., Electrostatic Interactions of a Solute with a Continuum. a Direct Utilization of Ab Initio Molecular Potentials for the Prevision of Solvent Effects, *Theor. Chem. Acc*., **103**: 343-345 (2000).

[52] Okulik N., Jubert A.H., Theoretical Analysis of the Reactive Sites of Non-Steroidal Anti-Inflammatory Drugs, *Int. Elect. J. Mol. Des.*, **4**: 17-30 (2005).

[53] Politzer P., Murray J.S., The Fundamental Nature and Role of the Electrostatic Potential in Atoms and Molecules, *Theor. Chem. Acc.*, **108**: 134-142 (2002).

[54] Sajan D., Joseph L., Vijayan N., Karabacak M., Natural Bond Orbital Analysis, Electronic Structure, Non-Linear Properties and Vibrational Spectral Analysis of L-Histidinium Bromide Monohydrate: a Density Functional Theory', *Spectrochim. Acta A*, **81**: 85-98 (2011).

[55] Hansch C., Leo A., Taft R.W., A Survey of Hammett Substituent Constants and Resonance and Field Parameters, *Chem. Rev.*, **91**: 165-195 (1991).

[56] Jensen L., Van Duijnen P.T., The First Hyperpolarizability of P-Nitroaniline In 1,4-Dioxane: a Quantum Mechanical/Molecular Mechanics Study, *J. Chem. Phys.*, **123**: Article ID 074307 (2005).

[57] Sałek P., Vahtras O., Helgaker T., Ågren H., Density-Functional Theory of Linear and Nonlinear Time-Dependent Properties Molecular, *J. Chem. Phys.*, **117**: 9630-9635 (2002).

[58] Stähelin M., Burland D.M., Rice J.E., Sign Change of Hyperpolarizabilities of Solvated Water, *Chem. Phys. Lett.*, **191**: 245-250 (1992)

[59] Huyskens F.L., Huyskens P.L., Persoons, A.P., Solvent Dependence of the First Hyperpolarizability of P-Nitroanilines: Differences Between Nonspecific Dipole–Dipole Interactions and Solute–Solvent H-Bonds, *J. Chem. Phys.*, **108**: 8161-8168 (1998).

[60] Zhang C.R., Chen H.S., Wang G.H., Geometry, Electronic Structure, and Related Properties of Dye Sensitizer: 3,4-Bis[1-(Carboxymethyl)-3-Indolyl]-1H-Pyrrole-2,5-Dione, *Chem. Res. Chin. U*, **20**: 640-646 (2004).

[61] Sun Y., Chen X., Sun L., Guo X., Lu W., A Monolayer Organic Light-Emitting Diode Using an Organic Dye Salt, *Chem. Phys. Lett.*, **83**: 1020-1022 (2003).

[62] Christiansen O., Gauss J., Stanton J.F., Non-Linear Optical Properties of Matter, *Chem. Phys. Lett.*, **305**: 51-99 (1999).

[63] Cheng L.T., Tam W., Stevenson S.H., Meredith G.R., Rikken G., Marder S.R., Experimental Investigations of Organic Molecular Nonlinear Optical Polarizabilities. 1. Methods and Results on Benzene and Stilbene Derivatives, *J. Phys. Chem.*, **95**: 10631-10643 (1991).

[64] Karna S.P., Prasad P.N., Dupuis M., Nonlinear Optical Properties of Novel Thiophene Derivatives: Experimental and Ab Initio Time-Dependent Coupled Perturbed Hartree–Fock Studies, *J. Chem. Phys.*, **94**: 1171-1179 (1991).

[65] Kaatz P., Donley E. A., Shelton D.P., A Comparison of Molecular Hyperpolarizabilities from Gas and Liquid Phase Measurements, *J. Chem. Phys.*, **108**: 849-855 (1998).